Enhancing the Adsorption Performance of 2-Methylisoborneol by Activated Carbon by Promoting Hydrophobic Effects

Fan Yang,[a, c] Jianwei Yu,*, [a, c] Qi Wang,[a, c] Chunmiao Wang,[a] Yuning Du,[a] Zhiyuan Liu,[a, c] Lili Zhang,[a, c] Zhengang Liu,[b, c] C Jing,[a, c] Junwang Tang,[d] and Min Yang,*, [a, c]

[a] F. Y, Prof. Dr. J. W. Y, Q. W, C. M. W, Y. N. D, Z. Y. L, Prof. Dr. M. Y
Key Laboratory of Drinking Water Science and Technology, Research Center for Eco-Environmental Sciences
Chinese Academy of Sciences
18 Shuangqing road, Beijing 100085 (China)
E-mail: jwyu@rcees.ac.cn
yangmin@rcees.ac.cn

[b] Prof. Dr. Z. G. L
Department of Solid Waste Treatment and Recycling, Research Center for Eco-Environmental Sciences
Chinese Academy of Sciences
18 Shuangqing road, Beijing 100085 (China)

[c] F. Y, Prof. Dr. J. W. Y, Q. W, Z. Y. L, Prof. Dr. Z. G. L, J. C. Prof. Dr. M. Y
University of the Chinese Academy of Sciences
19 Yuquan Road, Beijing 100049 (China)

[d] Prof. Dr. J. W. T
Department of Chemical Engineering
University College London
Torrington Place, London, WC1E 7JE (UK)

Abstract: Increasing the adsorption capacity of activated carbon, which is the most widely used adsorbent in drinking water treatment, is an attractive option for reducing the cost and production of sludge. In this study, we attempted to increase the adsorption capacity of activated carbon to 2-methylisobornel (MIB), a typical odorant in drinking water, through catalytic graphitization using $Fe(NO_3)_3$ as the catalyst. The graphitization degrees of five commercial powered activated carbon (PAC) products with different origins (wood, coal, or coconut shell) were increased by 16.04%–27.98% after catalytic graphitization, resulting in a 2.47–3.00-fold increase in q_{10} (adsorption amount at equilibrium MIB concentration of 10 ng L^{-1}, ng mg^{-1}) compared to the original ones. Formation of graphitized planar networks were identified via transmission electron microscopy (TEM), showing clear lattice fringes with 5–7 oriented layers spaced at 0.3404 nm. The increase in graphitization degrees was supported by Raman spectroscopy, which showed a 12%–32% decrease in the intensity ratio of the D (1 340 cm^{-1}) to G (1 595 cm^{-1}) bands. X-ray photoelectron spectroscopy indicated that the ratio of the sp^2-hybridized carbon to the sp^3-hybridized one increased by 31.9%–49.8%, leading to the enhancement of hydrophobic interactions between the carbon surface and MIB molecules. Both the Fourier-transform infrared spectroscopy (FT-IR) and Boehm titration results showed that the contents of oxygen-containing functional groups decreased after graphitization. Reactive force field molecular dynamics (ReaxFF MD) and washburn method indicated that the surface of PGCs had stronger repulsion for water molecules, and MIB molecules tended to be adsorbed in the ordered graphitic moiety composed of hexatomic rings. This study provides a novel approach to develop high-performance activated carbon and improves our understanding of adsorption mechanisms.

Introduction

Activated carbon, a typical amorphous carbon with a disordered and irregular microcrystalline layer structure,[1] is widely used in drinking water treatment for the removal of micropollutants.[2] Dosing powdered activated carbon (PAC) is a major approach to resolve the seasonally occurring taste and odor problems by removing pollutants such as 2-methylisobornel (MIB) and geosmin.[3] The adsorption capacity of PAC to MIB is quite limited, and thus a large amount of PAC will have to be dosed into water to remove MIB produced from cyanobacteria outbreak, resulting in the high cost, production of large amount of sludge, and the possible clogging of sand filters. Thus, the development of activated carbon with high adsorption capacity is becoming increasingly important to cope with the challenges.[4]

The highly developed pore structure of activated carbon allows pollutant molecules to diffuse into its internal pores and adhere to the surface.[5] Most adsorption occurs on the surface of the micropores, and pore-filling has been considered to be the primary mechanism for the adsorption of small-molecular organics by activated carbon.[6] MIB tends to be adsorbed on the interior surfaces of carbon pores through a physical mechanism due to its hydrophobic properties.[7] Previous studies have shown that the MIB adsorption capacity is positively correlated with the micropore volume of PAC. For example, the adsorption capacity of MIB on the PAC with a micropore volume of 0.45 cm^3 g^{-1} was 4.5 times that on the one with a micropore volume of 0.25 cm^3 g^{-1}.[8] However, the micropore volume of PAC can not be increased without limitation.[9] Therefore, the development of high-performance activated carbon for MIB removal relies on the discovery of other adsorption mechanisms.

The recent development of carbon nanomaterials (e.g., graphenes and carbon nanotubes) with highly active surfaces, strong quantum effects, and open-up layer morphology has attracted wide attention because of their excellent adsorption performance for small-molecule organics.[10] The high adsorption

capacity of these carbon nanomaterials may be attributed to the enhanced π-π or hydrophobic interaction between the adsorbate and the adsorbent, resulting from the highly ordered structure of the adsorbent in which carbon atoms are regularly arranged in a hexagonal pattern.[11] However, application of these novel carbon nanomaterials in water treatment is challenging because of their high cost, irreversible aggregation, and possible ecological risks.[12] Theoretically, carbon allotropes can be transformed by altering the periodic motifs in carbon atom networks due to their versatile flexibility.[10d, 13] Thus, it is assumed that the adsorption capacity of activated carbon may be increased if the surface amorphous carbon is reconstructed into the carbon atom networks with ordered arrangement. Typically, the order degree of activated carbon can be increased by converting the disordered carbon into a layered structure, i.e., increasing the ratio of graphite crystallites.[11b, 14] In general, graphitization requires heating of carbon materials at a high temperature (>2 500 ℃), which could be greatly decreased in the presence of catalysts.[15]

In this study, porous graphitized carbons (PGC) were successfully obtained through catalytically graphitizing the PAC products of different origins (wood, coal, or coconut shell) at a low calcination temperature using $Fe(NO_3)_3$ as the catalyst. The MIB adsorption capacities and physicochemical properties of the carbon adsorbents before and after graphitization were evaluated. Changes in carbon structure were characterized using multi-technologies including high-resolution transmission electron microscopy (HR-TEM), X-ray diffraction (XRD), Raman spectroscopy, X-ray photoelectron spectroscopy (XPS), Fourier-transform infrared spectroscopy (FT-IR) and Boehm titration. The adsorption mechanism was explored in combination with reactive force field molecular dynamics (ReaxFF MD) and washburn method. This study provides a novel approach to develop high-performance activated carbon for MIB removal and improves our understanding of adsorption mechanisms of carbon materials.

Results and Discussion

MIB adsorption performance. The MIB adsorption isotherms of different carbon adsorbents before and after graphitization are shown in Figure 1. Similar to previous studies,[16] MIB adsorption was well expressed with the Freundlich isotherm model, which was used to calculate q_{10} (equilibrium adsorption at Ce of 10 ng L^{-1}, ng mg^{-1}) to represent the adsorption capacity of the adsorbent, as shown in Table 1. The MIB adsorption capacities increased greatly after catalytic graphitization of PAC, and the corresponding q_{10} values increased by 2.47–3.00 times. The five pristine PAC adsorbents before graphitization showed correlations between MIB adsorption capacity and micropore volume (Spearman rank correlation coefficient: r = 0.90, p = 0.04), in accordance with previous research.[8]

Table1. Characteristics of activated carbon products before and after graphitization.

Adsorbent[a]	q_{10}[c] (ng mg^{-1})	SBET (m^2 g^{-1})	Vtot (cm^3 g^{-1})	Vmic (cm^3 g^{-1})	Basic site (mmol L^{-1})	Acidic site (mmol L^{-1})	Phenolic group (mmol L^{-1})	Carboxyl group (mmol L^{-1})	Lactonic group (mmol L^{-1})
W	389.84	1250.53	0.7850	0.4369	0.5173	0.4790	0.2499	0.1482	0.0810
W-G[b]	1048.64	1265.64	0.8420	0.4176	0.4951	0.1608	0.0814	0.0558	0.0235
Coa	372.57	1093.31	0.4840	0.4140	0.4157	0.3630	0.1375	0.1482	0.0773
Coa-G[b]	922.07	1094.76	0.5100	0.4029	0.3787	0.1982	0.0713	0.0787	0.0483
Coc1	366.41	1119.04	0.4700	0.4179	0.5635	0.3854	0.1298	0.1482	0.1075
Coc1-G[b]	984.88	1094.44	0.4820	0.4160	0.5143	0.2764	0.0936	0.1032	0.0796
Coc2	252.39	857.97	0.4954	0.3493	0.4896	0.4416	0.2222	0.1703	0.0491
Coc2-G[b]	693.34	888.86	0.5088	0.3455	0.3233	0.1308	0.0651	0.0502	0.0155
Coc3	159.57	429.08	0.3971	0.1336	0.5229	0.3480	0.1575	0.1666	0.0238
Coc3-G[b]	478.15	426.83	0.3740	0.1229	0.4862	0.1587	0.0783	0.0462	0.0342

[a] Carbon materials made from wood (W), coal (Coa) and coconut (Coc). [b] Carbon materials after graphitization. [c] Equilibrium adsorption amount at Ce of 10 ng L^{-1}.

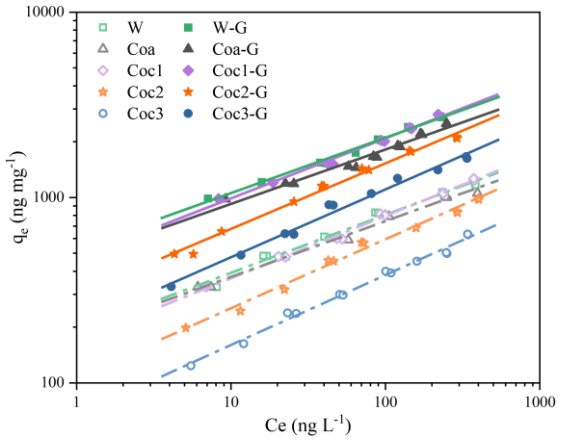

Figure 1. Adsorption isotherms of MIB onto PACs and PGCs at initial concentration of 500 ng mg^{-1}.

After catalytic graphitization, no significant changes in terms of S_{BET} (-2.2%–3.60%), V_{tot} (-5.82–7.26%), and V_{mic} (-8.01%–0.47%) were observed for the tested adsorbents (Table 1). MIB molecules are composed of a hydrocarbon skeleton containing a hydroxyl group, the kinetic diameter of which is ~0.6 nm [17]. Previous studies have reported that the $V_{(0.9–1.2\ nm)}$ is significantly correlated with MIB removal.[2b, 18] Thus, changes in micropores were analyzed in detail (Figure S2). For the five adsorbents, the volumes of micropores below 0.6 nm ($V_{<0.6\ nm}$, cm^3 g^{-1}) decreased by 11.98%–41.48%, whereas the volumes of micropores between 0.9 and 1.2 nm ($V_{0.9–1.2\ nm}$, cm^3 g^{-1}) increased by 10.70%–13.33%. However, the limited increase in $V_{(0.9–1.2\ nm)}$ could not explain the significant increase in the MIB adsorption capacities caused by graphitization.

Changes in morphological and crystal microstructure after catalytic graphitization. Changes in the morphological structure via catalytic graphitization of a coconut shell PAC (Coc1 and Coc1-G) were observed using HR-TEM, as shown in Figure 2. Coc1 exhibited a disordered structure and random orientation, while Coc1-G exhibited clear lattice fringes with 5–7 oriented layers spaced at 0.3404 nm. Graphite is known to have a layer spacing of 0.3354 nm.[19] During catalytic graphitization, the added ferric nitrate might have been transformed into iron particles and melted to form liquid Fe-C droplets on the PAC surface with graphite gradually precipitating from the molten iron

to form graphene layers.[20] Due to the associated decrease in free energy, the surface amorphous carbon structure of PAC was partially transformed into graphitized planar networks to form PGC.

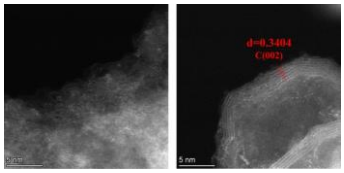

Figure 2. HR-TEM images of adsorbents before and after graphitization (left, Coc1 ; right, Coc1-G).

Changes in the crystal structure of the PACs were investigated using XRD (Figure 3). The patterns of all samples contained an intense peak centered at approximately 26.5° corresponding to the 002 plane of graphite.[21] In accordance with the occurrence of graphene layers observed by HR-TEM, movement towards a higher Bragg angle (Table S2) and increase in the 002 peak intensity of the PGCs were observed following graphitization.[19]

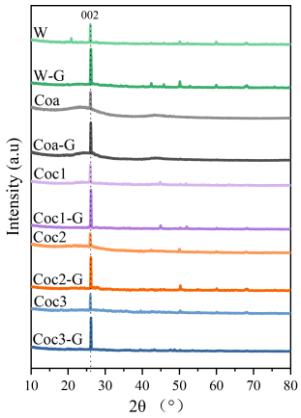

Figure 3. XRD patterns of PACs and PGCs.

Calculation of the crystal layer spacing of (002) ($d_{(002)}$, nm) and graphitization degree (g, %) of the adsorbents are shown in Table S2. It was clear that the graphite structure existed in the pristine commercial PACs but the proportion were low (11.20%~19.76%). After catalytic graphitization, the graphitization degrees of all five PACs increased to 35.81%–41.77%, and the layer spacing ($d_{(002)}$) decreased from 0.3423–0.3427 nm to 0.3404–0.3410 nm. These results were consistent with the HR-TEM results, showing that the layer spacing of the acquired PGCs was closer to that of graphite (0.3354 nm).[19] Compared with the coal origin PAC (1.82 times), the wood and coconut origin PACs exhibited larger increases in graphitization degree (2.48–2.78 times), which might be attributed to the higher activity of iron in the wood and coconut origin PACs with the breaking of C-H, C-O, and other bonds.[15a] Consistent with the graphitization degree changes, the q_{10} of the wood and coconut origin PGCs (W-G and Coc-G) increased by 2.69–3.00 times compared to that of the coal origin one (Coa-G) (2.47 times), suggesting a significant influence of graphitization degree on adsorption capacity (Spearman rank correlation coefficient: r = 0.72, p = 0.02).

The increases in graphitization degrees were further confirmed by Raman spectroscopy, as shown in Figure 4 (a). Two Raman peaks were identified at 1 340 cm^{-1} (D-band) and 1 595 cm^{-1} (G-band), respectively. The D band was caused by Raman A_{1g} in-plane breathing vibration, representing a defective graphite structure or disordered carbon owing to the presence of the sp^3-hybridised carbon, whereas the G band was generated by Raman active E_{2g} in-plane vibration of the sp^2-hybridised bonds in the bonded hexagonal lattice of graphitic carbon.[22] The intensity ratio of the D to G bands (I_D/I_G) was obtained for each adsorbent by fitting the Gaussian line shape, as shown in Figure 3 (c). The I_D/I_G values decreased by 12%–32% after catalytic graphitization, indicating that the ordered carbon structure proportion in the materials increased.[23]

XPS spectra with binding energies from 200 to 900 eV were acquired, as shown in Figure 4 (b). The C1s spectra were deconvoluted to seven peaks using the Gaussian-Lorentzian line, as shown in Figure 4 (c, d) and Figure S3 (a-d). The full width half-maximum (FWHM) was set to 1.1–2 eV for the C–C peaks, while the C-O and π-π* peaks were set to 1.8–2.2 eV and 2–3 eV, respectively.[15c, 21, 24] The C-C peaks were classified into primary, high, and low peaks, which were assigned to the sp^2-hybridized carbon in aromatic structure at 284.4 eV, the sp^3-hybridized carbon in disordered phase at 285 eV, and the second class of defective carbon at 284 eV, respectively.[25] The oxygenated region was ascribed to three curves centered at 286.2 eV (C-O), 287.5 eV (C=O), and 289 eV (O-C=O), respectively.[25c] The C-C (primary) proportion increased by 7.90%–18.32%, while the C-C (high) proportion decreased by 14.47%–26.77% after catalytic graphitization (Table S3). At the same time, the sp^2/sp^3 ratio represented by C-C (primary)/C-C (high) increased by 31.93%–49.84%. Thus, the XPS results also indicated enhancement of the ordered graphite structure in PGCs.[26]

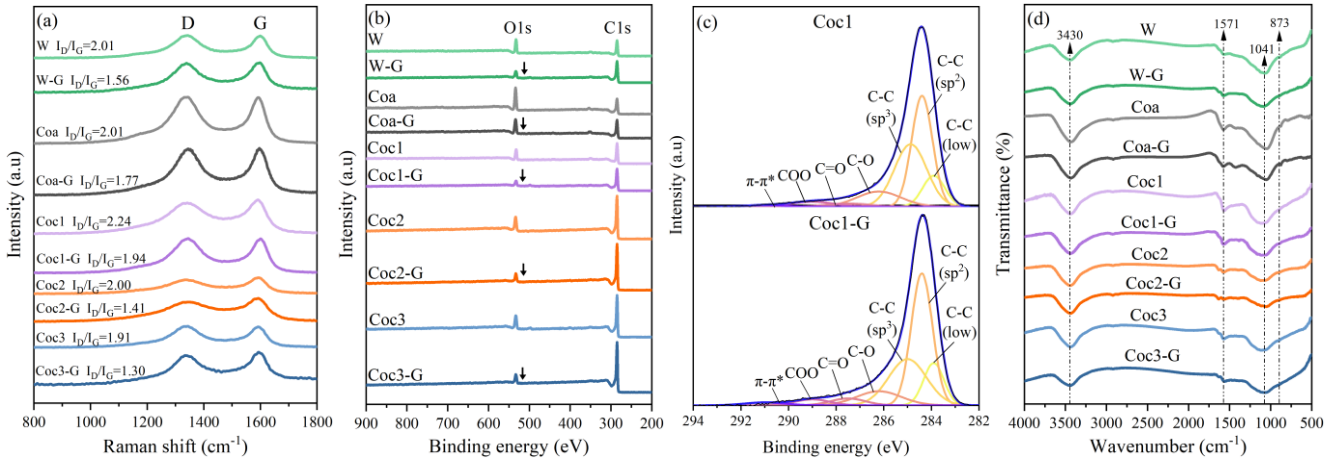

Figure 4. (a) Raman patterns and I_D/I_G values of PACs and PGCs，(b) XPS spectra of PACs and PGCs, (c) C1s spectrum of Coc1 and Coc1-G, (d) FTIR spectra of PACs and PGCs.

Changes in surface chemical properties after catalytic graphitization. In addition, the XPS analysis revealed the oxygen content decreased by 4.71%–8.63% after graphitization (Table S3). Consistently, the reduction in oxygen-containing groups was supported by FT-IR spectroscopy. In the FT-IR spectroscopy (Figure4 (d)), the peaks at 3 430 cm^{-1}, 1 571 cm^{-1}, 1 041 cm^{-1}, and 873 cm^{-1} were assigned to O-H stretching vibration,[27] C=C skeleton vibration,[28] C-O-C symmetrical stretching vibration, and benzene ring CH in-plane deformation,[29] respectively. All vibration peaks were slightly weakened after graphitization treatment, indicating a decrease in oxygen-containing functional groups. Most oxygen-containing groups on the PAC surface have acidic properties.[30] The Boehm titration results showed that the contents of all acidic sites, including the carboxylic, lactonic, and phenolic groups, decreased visibly (28.28%–70.38%) after graphitization (Table 1). Previous studies have shown that an increase in acidic functional groups on the carbon surface will lead to an increase in water molecule adsorption,[31] which may block pores and prevent MIB molecules from entering the adsorption sites.[32] Therefore, the decrease in acidic functional groups on the carbon surface should also be favorable for the adsorption of MIB.

Adsorption behavior of MIB in aqueous solution. In graphite crystallites, each sp^2-hybridized carbon atom is assumed to be connected with three other carbon atoms, with six carbon atoms then forming a regular hexagonal ring on the same plane extending to form an ordered graphite microcrystalline lamellar structure.[33] Therefore, a graphene plane containing oxygen-containing functional groups and structural defects was designed to simulate the adsorption process of MIB on the surface of activated carbon in the aqueous solvent model using ReaxFF MD simulation. The effects of oxygen-containing functional groups (one carboxyl (-COOH), one ester (-COOC -), one epoxyl (-O-) and two hydroxyl (-OH) groups) and disordered states (vacancy and Schweil defect) on MIB adsorption were investigated.

As shown in Figure 5, MIB molecules tend to adsorb on the sites of the hexatomic ring, while the defective regions on the activated carbon surface are all occupied by water molecules. Polar molecules are more likely to attach to defects due to the effect of dipoles or hydrogen bonds. In this study, the defect sites are more likely to adsorb water molecules, which may block channels and negatively affect MIB adsorption. After catalytic graphitization, the increase of ordered graphitic structure composed of the sp^2 carbon and the reduction of defects lead to the conversion of sites easily occupied by water into the ones that are easily adsorbed by MIB, which was reflected in the improvement of adsorption capacity.

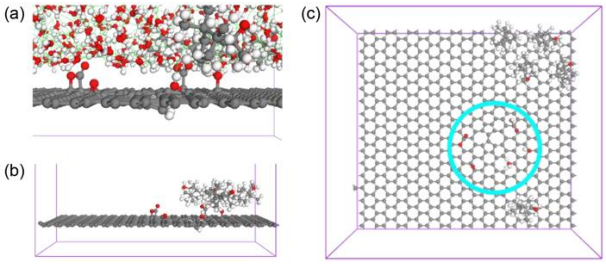

Figure 5. The resulted adsorption state of H_2O molecules (a) and MIB molecules (b and c, front and top views) on the graphite surface model with oxygen-containing functional groups and structural defects. C atoms shown in grey, O in red, and H in white. The cyan circle can guide the eyes to the defect domain.

The adsorption of solids in solution is complicated. In addition to the influence of solvent, the adsorption behavior is also affected by the interaction between adsorbent and adsorbate. It is known that the graphitic materials consisting of the naturally existing sp^2 carbon are hydrophobic, with a water contact angle of ~90° and a low surface energy.[34] Previous literatures have demonstrated that the ordered crystalline-like hydrophobic surface exhibits stronger hydrophobic attraction than the disordered liquid-like hydrophobic surface due to the water structure effect, and the multi-layer graphite structure is more hydrophobic than the single-layer graphene.[35]

Therefore, the contact angles and surface energy of the carbon adsorbents before and after catalytic graphitization were determined using the washburn method, as shown in Table 2. The surface energy of carbon materials tends to decrease after catalytic graphitization (26.67%-36.40%), indicating higher hydrophobicity of PGCs, which was favorable for the low polarity MIB molecules (log KOW = 3.31) to adsorb to the interior of the carbon pores via hydrophobic interactions.

Table 2. Contact angles and surface energies of PACs and PGCs.

PAC/PGC	$\theta_{c\text{-Water}}$ (°)	$\theta_{c\text{-Formamide}}$ (°)	$\theta_{c\text{- Decane}}$ (°)	Surface energy (mN m^{-1})	Dispersive component (mN m^{-1})	Polar component (mN m^{-1})
W/W-G	69.2/81.4	65.9/77.6	80.0/82.8	34.15/24.01	8.08/7.43	26.07/16.58
Coa/Coa-G	63.2/72.9	69.1/83.3	55.9/59.4	34.75/26.09	12.74/11.21	22.02/14.88
Coc1/Coc1-G	69.1/81.0	67.3/84.1	71.8/74.2	32.83/22.26	9.80/8.59	23.04/13.67
Coc2/Coc2-G	66.3/78.2	67.2/83.9	65.1/67.3	34/23.48	11.11/9.89	22.88/13.59
Coc3/Coc3-G	66.2/81.9	65.0/76.4	73.3/77.1	35.48/23.12	9.41/8.50	26.07/14.62

And we found an interesting phenomenon: both the contact angles of the polar (water and formamide) and non-polar molecules (decane) increased. However, the increases in the contact angles for the polar molecules (15.35%-23.72% for water, 17.54%-24.96% for formamide) were much more significant than that for the non-polar molecule (3.34%-6.26% for decane).The total solid surface energy was further divided into the dispersive and polar components according to the Fowkes/Owens-Wendt interface interaction theory, which represent the non-polar and polar components of the surface, respectively.[36] After the catalytic graphitization, the dispersive and the polar components decreased by 8.04%-12.35% and 32.43%-43.92%, respectively. The larger decrease of the polar component on the carbon surface means the reduction of the adsorption potential to the polar water molecules, leaving more adsorption sites for MIBs. This result was in accordance with the ReaxFF MD simulation result. Thus the increased hydrophobicity of PGCs resulted in stronger repulsion to water molecules, leaving more sites for the adsorption of MIB.

Conclusion

In this study, catalytic graphitization of five PACs using $Fe(NO_3)_3$ as the catalyst was tried to increase their MIB adsorption performance. The graphitization degrees of the five PACs with different origins (wood, coal, or coconut shell) were increased by 16.04%–27.98% through catalytic graphitization, resulting in a 2.47–3.00-fold increase in q_{10} (adsorption amount at equilibrium MIB concentration of 10 ng L^{-1}, ng mg^{-1}) compared to the original ones. Increased repulsion for water molecules makes graphitized PAC to exhibit significantly increased MIB adsorption capacity. After catalytic graphitization, the hydrophobicity of the activated carbon surface increased significantly because of the increased ordered graphitic structure and the reduction of defects, making it to exhibit stronger repulsion for water molecules, and leave more sites for MIB. This study could provide guidance for improving the adsorption performance of PAC for the removal of other pollutants.

Acknowledgements

The research was supported by the Funds for the National Natural Science Foundation of China (52070185; 52100018), National Key R&D Program of China (2021YFC3200904), the fellowship of China Postdoctoral Science Foundation (2020M680709) and Excellent Innovation Project of Research Center for Eco-Environmental Sciences, CAS (RCEES-EEI-2019-02).

Keywords: activated carbon • graphited porous carbon • catalytic graphitization • MIB adsorption • hydrophobicity

[1] a) Y. Zhai, W. Ying, C. Yan, Y. Shi, F. Zhang, T. Bo, D. Zhao, *Journal of Porous Materials* **2008**, *15*, 601-611; b) J. M. Carlsson, *Simulations of the Structural and Chemical Properties of Nanoporous Carbon*, Computer-Based Modeling of Novel Carbon Systems and Their Properties, **2010**.

[2] a) W. Bunmahotama, W. N. Hung, T. F. Lin, *Water Research* **2017**, *111*, 28-40; b) P. Pendleton, S. H. Wong, R. Schumann, G. Levay, J. Rouquero, *Carbon* **1997**, *35*, 1141-1149.

[3] a) J. Yu, F.-C. Yang, W.-N. Hung, C.-L. Liu, M. Yang, T.-F. Lin, *Chemosphere* **2016**, *156*, 374-382; b) D. Cook, G. Newcombe, P. Sztajnbok, *Water research* **2001**, *35*, 1325-1333.

[4] a) M. Pivokonsky, I. Kopecka, L. Cermakova, K. Fialova, K. Novotna, T. Cajthaml, R. K. Henderson, L. Pivokonska, *Science of The Total Environment* **2021**, *799*, 149455; b) L. F. Delgado, P. Charles, K. Glucina, C. Morlay, *Science of The Total Environment* **2012**, *435-436*, 509-525.

[5] **!!! INVALID CITATION !!! [6]**.

[6] a) Haul, R., *Zeitschrift Für Physikalische Chemie* **1969**, *63*, 220-221; b) J. E. Lennard-Jones, *Transactions of the Faraday Society* **1932**, *28*; c) M., Jaroniec, *Advances in Colloid & Interface Science* **1983**.

[7] a) Y. Matsui, S. Nakao, A. Sakamoto, T. Taniguchi, L. Pan, T. Matsushita, N. Shirasaki, *Water Res* **2015**, *85*, 95-102; b) M. F. Tennant, D. W. Mazyck, *Carbon* **2007**, *45*, 858-864.

[8] J. Yu, M. Yang, T. Lin, Z. Guo, Y. Zhang, J. Gu, S. Zhang, *Separation and Purification Technology* **2007**, *56*, 363-370.

[9] J. Alcañiz-Monge, in *Studies in Surface Science and Catalysis, Vol. 144* (Eds.: F. Rodriguez-Reinoso, B. McEnaney, J. Rouquerol, K. Unger), Elsevier, **2002**, pp. 193-200.

[10] a) G. Ersan, O. G. Apul, F. Perreault, T. Karanfil, *Water Research* **2017**, 385; b) K. S. Novoselov, V. I. Fal'Ko, L. Colombo, P. R. Gellert, K. A. Kim, *Nature* **2012**, *490*, 192-200; c) M. D. Volder, S. H. Tawfick, R. H. Baughman, A. J. Hart, *Science* **2013**, *339*, 535-539; d) B. Ywa, B. Pya, B. Lza, B. Xsa, B. Hza, *Energy Storage Materials* **2020**, *26*, 349-370.

[11] a) J. Biscoe, B. E. Warren, *Journal of Applied Physics* **1942**, *13*, 364-371; b) M. M. Haley, *Pure and Applied Chemistry* **2008**; c) Y. Ding, M. Zeng, L. Fu, *Science Bulletin* **2019**, *64*, 1817-1829.

[12] a) Y. Lin, Y. Tian, H. Sun, T. Hagio, *Chemosphere* **2020**, *270*, 129420; b) Y. Ren, F. Yu, X.-G. Li, J. Ma, *Materials Today Chemistry* **2021**, *22*, 100603; c) J. Zhao, Z. Wang, J. C. White, B. Xing, *Environmental Science & Technology* **2014**, *48*, 9995-10009.

[13] P. Rivera-Fuentes, F. Diederich, *Angewandte Chemie* **2012**.

[14] F. Diederich, M. Kivala, *Advanced Materials* **2010**, *22*, 803-812.

[15] a) Yan, Qiangu, Li, Jinghao, Zhang, Xuefeng, Hassan, El, Barbary, Wang, *Journal of Nanoparticle Research An Interdisciplinary Forum for Nanoscale Science & Technology* **2018**; b) D. Zhai, H. Du, B. Li, Y. Zhu, F. Kang, *Carbon* **2011**, *49*, 725-729; c) F. Destyorini, R. Yudianti, Y. Irmawati, A. Hardiansyah, Y.-I. Hsu, H.

Uyama, *Diamond and Related Materials* **2021**, *117*, 108443.
[16] a) T. Bong, J.-K. Kang, V. Yargeau, H.-L. Nam, S.-H. Lee, J.-W. Choi, S.-B. Kim, J.-A. Park, *Journal of Cleaner Production* **2021**, *314*, 127967; b) Y. Matsui, S. Nakao, T. Taniguchi, T. Matsushita, *Water Res* **2013**, *47*, 2873-2880.
[17] R. Considine, R. Denoyel, P. Pendleton, R. Schumann, S. H. Wong, *Colloids & Surfaces A Physicochemical & Engineering Aspects* **2001**, *179*, 271-280.
[18] a) L. Lei, P. A. Quinlivan, D. Knappe, *Carbon* **2002**, *40*, 2085-2100; b) G. Newcombe, M. Drikas, R. Hayes, *Water Research* **1997**, *31*, 1065-1073.
[19] H. Li, H. Zhang, K. Li, J. Zhang, M. Sun, B. Su, *Fuel* **2020**, *279*, 118531.
[20] a) S. Xia, N. Cai, J. Wu, H. Xiao, J. Hu, X. Chen, Y. Chen, H. Yang, X. Wang, H. Chen, *Fuel Processing Technology* **2020**, *209*, 106543; b) R. R. Bacsa, I. Cameán, A. Ramos, A. B. Garcia, V. Tishkova, W. S. Bacsa, J. R. Gallagher, J. T. Miller, H. Navas, V. Jourdain, M. Girleanu, O. Ersen, P. Serp, *Carbon* **2015**, *89*, 350-360; c) J. A. Rodríguez-Manzo, C. Pham-Huu, F. Banhart, *ACS Nano* **2011**, *5*, 1529-1534.
[21] F. Destyorini, Y. Irmawati, A. Hardiansyah, H. Widodo, I. N. D. Yahya, N. Indayaningsih, R. Yudianti, Y.-I. Hsu, H. Uyama, *Engineering Science and Technology, an International Journal* **2021**, *24*, 514-523.
[22] a) J. Dennison, M. Holtz, *Spectroscopy (Santa Monica)* **1996**, *11*, 38-46; b) W. Guan, Y. Wang, C. B. Fischer, S. Wehner, Z. Wang, J. Li, C. Wang, W. Guo, Q. Xue, *Applied Surface Science* **2020**, *505*, 144626; c) D. Janke, F. Munnik, J. Julin, R. Hübner, J. Grenzer, C. Wüstefeld, S. Gemming, D. Rafaja, M. Krause, *Carbon* **2020**, *159*, 656-667; d) Y. Kang, B. Li, J. Zhao, B. Ge, M. Weng, Z. Shi, Y. Zhao, *Vacuum* **2020**, *172*, 109043.
[23] A. C. Ferrari, *Phys. Rev. B* **2000**, *61*.
[24] R. Blume, D. Rosenthal, J.-P. Tessonnier, H. Li, A. Knop-Gericke, R. Schlögl, *ChemCatChem* **2015**, *7*, 2871-2881.
[25] a) H. Estrade-Szwarckopf, *Carbon* **2004**, *42*, 1713-1721; b) S. T. Jackson, R. G. Nuzzo, *Applied Surface Science* **1995**, *90*, 195-203; c) M. Smith, L. Scudiero, J. Espinal, J.-S. McEwen, M. Garcia-Perez, *Carbon* **2016**, *110*, 155-171.
[26] N. Shimodaira, A. Masui, *Journal of Applied Physics* **2002**, *92*, 902-909.
[27] J. Wang, B. Chen, B. Xing, *Environ Sci Technol* **2016**, *50*, 3798-3808.
[28] Y. Shao, J. Li, X. Fang, Z. Yang, Y. Qu, M. Yang, W. Tan, G. Li, H. Wang, *Chemosphere* **2022**, *287*, 132118.
[29] a) H. Yuan, T. Lu, Y. Wang, H. Huang, Y. Chen, *Journal of Analytical and Applied Pyrolysis* **2014**, *110*, 277-284; b) X. Dong, L. Q. Ma, Y. Zhu, Y. Li, B. Gu, *Environ Sci Technol* **2013**, *47*, 12156-12164.
[30] a) Yang, T. Ralph, *Belgeler Com* **2003**, *2004*, xii,404; b) Francisco, V. c. ñas, and, Manuel, Fernando, R., Pereira, and, José, M. J., *Journal of Colloid & Interface Science* **2006**.
[31] a) W. Shen, Z. Li, Y. Liu, *Recent Patents on Chemical Engineeringe* **2008**, *1*, 27-40; b) S. S. Barton, M. Evans, J. Macdonald, *Langmuir* **1994**, *10*, 4250-4252; c) S. S. Barton, M. Evans, J. Holland, J. E. Koresh, *Carbon* **1984**, *22*, 265-272.
[32] M. F. Tennant, D. W. Mazyck, *Carbon* **2007**, *45*, 858-864.
[33] D. Mildner, J. M. Carpenter, *Journal of Non-Crystalline Solids* **1982**, *47*, 391-402.
[34] a) F. M. Fowkes, W. D. Harkins, *Journal of the American Chemical Society* **1940**, *62*, 3377-3386; b) Y. J. Shin, Y. Wang, H. Han, G. Kalon, H. Yang, *Langmuir the Acs Journal of Surfaces & Colloids* **2010**, *26*, 3798-3802; c) R. Raj, S. C. Maroo, E. N. Wang, *Nano Letters* **2013**, *13*, 1509-1515; d) H. Liu, L. Li, *Extreme Mechanics Letters* **2017**, S235243161630205X.
[35] a) L. Xie, D. Yang, Q. Lu, H. Zhang, H. Zeng, *Current Opinion in Colloid & Interface Science* **2020**, *47*, 58-69; b) M. Munz, C. E. Giusca, R. L. Myers-Ward, D. K. Gaskill, O. Kazakova, *ACS Nano* **2015**, *9*, 8401-8411.
[36] D. K. Owens, R. C. Wendt, *Journal of Applied Polymer Science* **1969**, *13*.

Entry for the Table of Contents

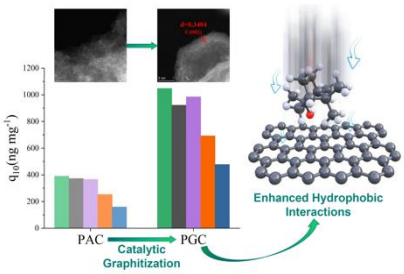

The MIB adsorption capacity of porous graphitized carbon (PGC) produced by catalytic graphitization was 2.47–3.00 times that of pristine powdered activated carbon (PAC), and its more ordered crystal structure enhanced hydrophobic interaction with MIB molecules to improves its adsorption capacity.